Dalton Transactions

ROYAL SOCIETY OF CHEMISTRY

PAPER

Cite this: *Dalton Trans.*, 2020, **49**, 15034

Synthesis of multifunctional metal–organic frameworks and tuning the functionalities with pendant ligands†

Thazhe Kootteri Prasad ‡ and Myunghyun Paik Suh *

Received 28th August 2020,
Accepted 5th October 2020

DOI: 10.1039/d0dt03012k

rsc.li/dalton

A series of multifunctional metal–organic frameworks (MOFs), **SNU-170–SNU-176**, has been synthesized using ligands, in which various functional pendants such as $-NH_2$, –SMe, –OMe, –OEt, –OPr, and –OBu are attached to the phenyl ring of 4-(2-carboxyvinyl)benzoic acid. The MOFs are isostructural but the interpenetration depends on the pendant group of the ligand. The MOFs exhibit high adsorption capacities for H_2, CO_2, and CH_4 gases, ligand-based photoluminescence, and chemical sensing abilities, all being affected by the pendant group. All of the as-synthesized MOFs can sense nitroaromatics by luminescence quenching, and some of the activated MOFs can sense the type of solvents by the altered emission maxima with enhanced intensity. In particular, **SNU-176** synthesized from a mixture of two different ligands with –SMe and –OMe pendants shows higher gas adsorption capacities than the MOFs synthesized from the individual ligands (**SNU-171** and **SNU-172**). It also shows the ability to differentiate nitrobenzene (NB) and 2,4-dinitrotoluene (DNT) unlike the MOFs composed of single ligands.

Introduction

The design and synthesis of metal–organic frameworks (MOFs) have attracted great attention due to the potential applications of MOFs in gas storage,[1–6] gas separation,[7,8] catalysis,[9–11] and chemical sensing.[12–14] It has been well known that the function of the MOFs can be tuned by the choice of metal and organic building blocks, but the strategy to generate multi-functionality in MOFs has been less explored.[15,16] Furthermore, despite numerous reports on luminescent MOFs, the application of them in chemical sensing is rather limited.[12,17,18] Here, we report the synthesis of multifunctional MOFs by using aromatic carboxylate ligands having functional organic pendants on the aryl ring. We previously reported versatile MOFs that have high surface areas and high gas uptake capacities;[6,19–22] one of which was **SNU-70** that was constructed from 4-(2-carboxyvinyl)benzoic acid (H_2CVB) and Zn^{2+} salt.[22] **SNU-70′** had an unusually high BET surface area (5290 $m^2\ g^{-1}$) and high H_2 and CO_2 gas-sorption capacities. To provide additional light-emitting and sensing properties to the MOFs, we have synthesized a series of ligands, H_2CVB-XR, where the phenyl ring of H_2CVB is functionalized with various electron-rich substituents such as $-NH_2$, –SMe, –OMe, –OEt, –OPr, and –OBu, and constructed new zinc(II) MOFs by using the ligands (Scheme 1). The resulting MOFs show multifunctional properties including high gas adsorption capacities, light-emitting properties in the visible region, and chemical sensing abilities for nitro-organics.

Results and discussion

Syntheses and X-ray crystal structures of SNU-170–SNU-176

We have synthesized a series of ligands, H_2CVB-XR, where XR is $-NH_2$, –SMe, –OMe, –OEt, –OPr, and –OBu (see the ESI†). By heating these ligands and $Zn(NO_3)_2{\cdot}6H_2O$ at 105 °C in *N*,*N*-dimethylformamide (DMF) for 24 h, we have obtained the MOF crystals of $[Zn_4O(CVB\text{-}NH_2)_3]{\cdot}18DMF{\cdot}H_2O$ (**SNU-170**), $[Zn_4O(CVB\text{-}SMe)_3]{\cdot}7DMF{\cdot}3H_2O$ (**SNU-171**), $[Zn_4O(CVB\text{-}OMe)_3]{\cdot}7DMF{\cdot}3H_2O$ (**SNU-172**), $[Zn_4O(CVB\text{-}OEt)_3]{\cdot}7DMF{\cdot}2H_2O$ (**SNU-173**), $[Zn_4O(CVB\text{-}OPr)_3]{\cdot}16DMF{\cdot}3H_2O$ (**SNU-174**), and $[Zn_4O$

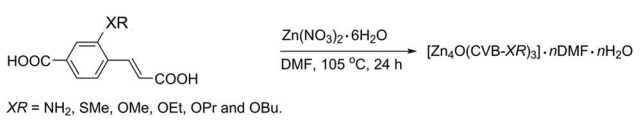

Scheme 1 Synthesis of MOFs from the functionalized 4-(2-carboxyvinyl)benzoic acids (H_2CVB-XR).

Department of Chemistry, Seoul National University, 1 Gwanak-ro, Gwanak-gu, Seoul 08826, Republic of Korea. E-mail: mpsuh@snu.ac.kr

†Electronic supplementary information (ESI) available. CCDC 1440326–1440330. For ESI and crystallographic data in CIF or other electronic format see DOI: 10.1039/d0dt03012k

‡Current address: Centre for Chemical Biology and Therapeutics, Institute for Stem Cell Science and Regenerative Medicine, Bellary Road, Bangalore 560 065, India.

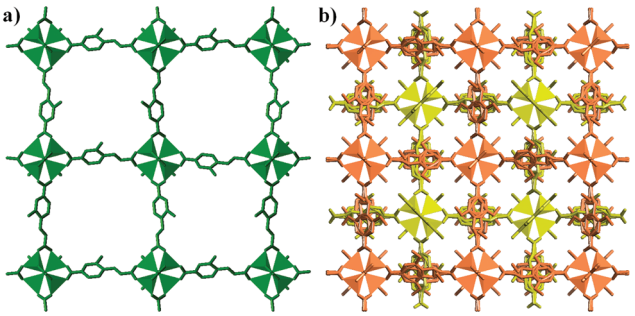

Fig. 1 X-ray crystal structures: (a) non-interpenetrated **SNU-170**; (b) doubly interpenetrated **SNU-171**. The disordered parts and pendant functional groups were modeled for clarity.

$(CVB\text{-}OBu)_3]\cdot 15DMF\cdot 3H_2O$ (**SNU-175**). Also, we have prepared $[Zn_4O(CVB\text{-}SMe)(CVB\text{-}OMe)_2]\cdot 7DMF\cdot 3H_2O$ (**SNU-176**) by using a mixture of H_2CVB-SMe and H_2CVB-OMe (ESI†).

Single crystal X-ray diffraction studies reveal that **SNU-170–SNU-174** have similar cubic-net structures consisting of $[Zn_4O]^{6+}$ octahedral building units and linear dicarboxylate linkers (Fig. 1 and Table S1, ESI†). In the crystal structures, the ligands were not well resolved due to the severe structural disorders and thus their average conformations are presented. The connections of the carboxylate groups of the ligand between the $[Zn_4O]$ units indicate that the phenyl ring and the vinyl group linked by a C–C single bond are located on the same plane. For **SNU-175** and **SNU-176**, single crystals of the quality for X-ray diffraction analysis could not be obtained, and their structures were confirmed by the PXRD patterns. **SNU-170** and **SNU-174** have non-interpenetrated structures, and **SNU-171–SNU-173** have doubly interpenetrated frameworks. Based on the PXRD patterns, **SNU-175** with the –OBu pendant has a similar structure to that of **SNU-174** with the –OPr pendant, and **SNU-176** incorporating both –SMe and –OMe pendants has a similar structure to that of **SNU-171** and **SNU-172** (Fig. S8, ESI†). The NMR spectrum of **SNU-176**, measured in DMSO-d_6/DCl, indicates that it contains about 33% –SMe and 66% –OMe pendant groups (Fig. S10, ESI†). The results reveal that the linker with a rigid group ($-NH_2$) produces a non-interpenetrated framework (**SNU-170**), whereas the linkers with the rather small and flexible functional groups such as –SMe, –OMe, and –OEt yield doubly interpenetrated frameworks. The linkers with flexible but bulkier substituents such as –OPr and –OBu result in non-interpenetrated structures to accommodate the bulky groups in the pores.

Gas sorption properties of SNU-170′–SNU-176′

We measured the adsorption isotherms of N_2, H_2, CO_2, and CH_4 gases after activating the crystals of **SNU-170–SNU-176** with supercritical CO_2 (Fig. 2 and Fig. S11, ESI†). The data are summarized in Table 1. The activated MOFs, **SNU-171′–SNU-174′**, and **SNU-176′** undergo structural transformations as revealed by the PXRD patterns showing the altered peak positions and peak heights compared with those of the as-synthesized MOFs (Fig. S2–S8, ESI†). On activation, non-interpenetrated **SNU-170′** and **SNU-175′** become amorphous, but regain crystallinity by immersion in DMF for 1 h (Fig. S9, ESI†). The N_2 adsorption isotherms of **SNU-170′–SNU-176′** indicate that non-interpenetrated **SNU-170′** has the highest BET (Langmuir) surface area, 3200 (3970) $m^2\ g^{-1}$, among the present MOFs. The BET surface areas of doubly interpenetrated **SNU-171′–SNU-173′** are significantly lower than that of **SNU-170′**, but higher than **SNU-174′** and **SNU-175′** that incorporate the bulky pendants, –OPr and –OBu, respectively. Doubly interpenetrated **SNU-171′–SNU-173′**, despite the smaller surface areas, show higher uptake capacities of H_2 gas at 77 K and 1 atm and CO_2 gas at 298 K and 1 atm, compared with those of the non-interpenetrated **SNU-170′** and **SNU-174′**. They adsorb 45–51 $cm^3\ g^{-1}$ (2.0–2.3 mmol g^{-1}) of CO_2 at 298 K and 1 atm, about a half, compared with the top 20 MOFs with high CO_2 adsorption capacity.[7] Interestingly, **SNU-176′** composed of two different ligands with –SMe and –OMe pendants shows higher adsorption capacities for H_2, CO_2, and CH_4 gases as well as higher BET surface area and DR pore volume than the MOFs composed of the respective individual ligands, **SNU-171′** and **SNU-172′**. In particular, the isosteric heats (Q_{st}) of H_2, CO_2, and CH_4 adsorption in **SNU-170′–SNU-176′**, which contain functional organic pendants, are significantly higher than those in **SNU-70′** having no pendant (Table 1). This indi-

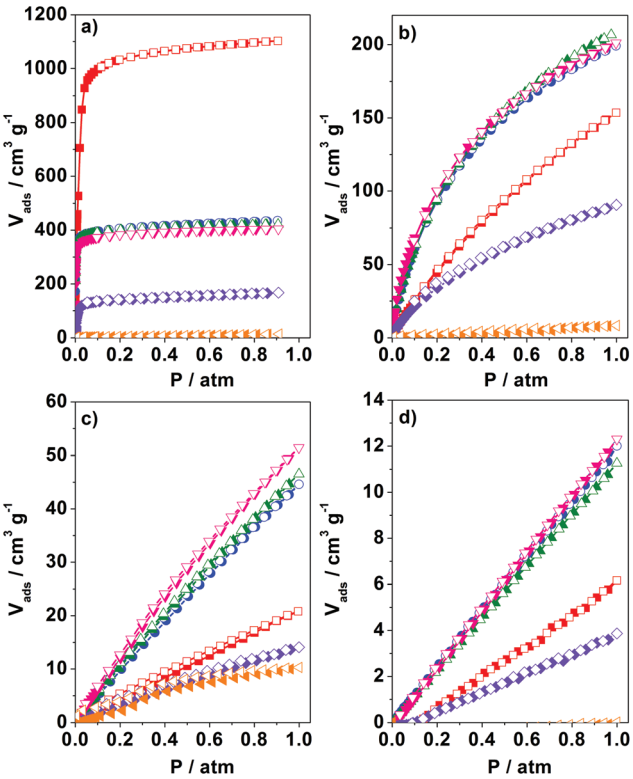

Fig. 2 Gas adsorption isotherms. (a) N_2 at 77 K, (b) H_2 at 77 K, (c) CO_2 at 298 K, and (d) CH_4 at 298 K. **SNU-170′** (red, square), **SNU-171′** (blue, circle), **SNU-172′** (green, triangle), **SNU-173′** (pink, inverted triangle), **SNU-174′** (violet, diamond), and **SNU-175′** (orange, rotated triangle). Filled shapes: adsorption; open shapes: desorption. For **SNU-176′**, see Fig. S11, ESI.†

Table 1 The gas adsorption properties of MOFs

	SNU-170′	SNU-171′	SNU-172′	SNU-173′	SNU-174′	SNU-175′	SNU-176′	SNU-70′
BET S.A. [$m^2\ g^{-1}$]	3200	1610	1600	1510	548	16	1780	5290
V_{pore} [$cm^3\ g^{-1}$]	1.24	0.67	0.64	0.61	0.27	—	0.74	2.17
H_2, 77 K[a] [$cm^3\ g^{-1}$]	154	199	207	201	91	8	235	134
H_2, 87 K[a] [$cm^3\ g^{-1}$]	81	131	132	135	59	7	141	78
Q_{st} (H_2)[b] [kJ mol^{-1}]	5.40	7.40	7.41	8.43	6.75	—	7.63	5.12
CO_2, 195 K[a] [$cm^3\ g^{-1}$]	361	374	363	353	244	62	413	1127
CO_2, 273 K[a] [$cm^3\ g^{-1}$]	39	96	91	97	29	13	101	31
CO_2, 298 K[a] [$cm^3\ g^{-1}$]	21	45	46	51	14	10	48	18
Q_{st} (CO_2)[c] [kJ mol^{-1}]	20.9	27	30.9	30.5	26.2	31.8	26.3	17.2
CH_4, 195 K[a] [$cm^3\ g^{-1}$]	36	189	166	175	54	—	186	54
CH_4, 273 K[a] [$cm^3\ g^{-1}$]	11	20	19	22	8	—	21	11
CH_4, 298 K[a] [$cm^3\ g^{-1}$]	6	12	11	12	4	—	12	7
Q_{st} (CH_4)[c] [kJ mol^{-1}]	—	18.7	16.6	23.1	—	—	17.4	9.4

[a] At 1 atm. [b] Isosteric heat of adsorption at zero coverage. [c] Isosteric heat of adsorption at low loading.

cates stronger interaction between the gases and the organic functional pendants of the MOFs. Furthermore, interpenetrated frameworks (**SNU-171′–SNU-173′**) exhibit higher Q_{st} (H_2, CO_2 and CH_4) values than the non-interpenetrated ones (**SNU-170′** and **SNU-174′**), similar to the other cases.[4,22]

To evaluate the CO_2 separation and capture ability of the present MOFs, the separation parameters[23] for the vacuum swing adsorption (VSA) process are calculated for the gas mixtures similar to flue gas (1 : 9 CO_2/N_2) and landfill gas (1 : 1 CO_2/CH_4) and summarized in Table S2, ESI.† The results indicate that **SNU-176′** is the best material among the present MOFs for flue gas separation by the VSA process (α_{12}^{ads} = 15.34 and S = 25.0). The characteristic pore properties generated from the two different functional groups (–SMe and –OMe) in **SNU-176′** might give rise to the phenomena.

Table 2 Photoluminescence properties of ligands and MOFs

	Ligands, nm			MOFs, nm	
	DMF solution[a]	Solid[b]		As-syn.[c]	Dried[c]
CVB-NH_2	493	525	**SNU-170**	512	536
CVB-SMe	478	499	**SNU-171**	471	482
CVB-OMe	404	460	**SNU-172**	412	442
CVB-OEt	405	432	**SNU-173**	413	440
CVB-OPr	406	430	**SNU-174**	412	442
CVB-OBu	405	420	**SNU-175**	414	440
CVB-SMe-OMe	—	—	**SNU-176**	472	470

[a] 1×10^{-4} M; excitation at 395 nm for H_2CVB-NH_2, 362 nm for H_2CVB-SMe, and 350 nm for the rest of the samples. [b] Excitation at 360 nm for H_2CVB-NH_2 and H_2CVB-SMe, and 320 nm for the rest of the samples. [c] Excitation at 400 nm for **SNU-170**, 390 nm for **SNU-171**, and 330 nm for the rest of the samples.

Photoluminescence properties of ligands and MOFs

The DMF solution of H_2CVB-NH_2 exhibits characteristic fluorescence in the visible region, which can be seen even by the naked eye, contrary to the non-emissive H_2CVB. Therefore, the photoluminescence (PL) properties of the H_2CVB-XR ligands and the MOFs are investigated. The PL emission spectra of the ligands (1×10^{-4} M) in the DMF solutions are significantly affected by the functional groups (Table 2 and Fig. S12, ESI†). The solutions of H_2CVB-XR with XR = NH_2 and SMe show the emission maxima that appear at significantly longer wavelengths, at 74–87 nm, than those with XR = OMe, OEt, OPr, and OBu. In the absence of an electron-donating group at the benzene ring of the ligand, the emission would be weak and takes place at a shorter wavelength (UV region), and hence is not shown in the visible region. For the ligands with the electron-donating substituents –XR, however, there exists more electron density in the benzene ring, and the emission takes place in the longer wavelength, visible region. The stronger the electron-donating nature of –XR, the longer the wavelength of the emission spectrum, XR = –NH_2 > –SMe > OR. The relative intensity of the emission spectrum of H_2CVB-NH_2 is about eight times stronger than that of H_2CVB-SMe and nearly twice stronger than those of H_2CVB-OR (R = Me, Et, Pr, Bu). The quantum yield of H_2CVB-NH_2 in DMF is 0.38, compared with 0.54 of quinine sulphate. For the other ligands, the quantum yields are too low to calculate with reliability. The solid-state PL spectra of the ligands show broader and red-shifted emission bands compared with those of the DMF solutions (Table 2), like the previous report.[24]

The as-synthesized MOFs are photoluminescent due to their luminescent ligands. The MOFs show red-shifted emission bands compared with those of the DMF solutions of the ligands, but blue-shifted emission bands compared with the corresponding solid ligands (Table 2). The emission shifts of the MOFs compared to the ligands may be related to the metal–ligand coordination that offers an electron-withdrawing effect on the ligand and/or the increased distance between the ligands in the MOF crystals, which affect the intra-ligand HOMO–LUMO energy gap.[25,26]

Upon the removal of DMF and H_2O guest solvent molecules from **SNU-170–SNU-176** by using supercritical CO_2, the resulting activated MOFs exhibit significantly decreased luminescence intensities of the red-shifted emission by 11 nm–30 nm, compared with the PL spectra of the as-synthesized MOFs (Table 2, Fig. 3, and Fig. S13, ESI†). A similar significant decrease in the emission intensity and the red-shift emission

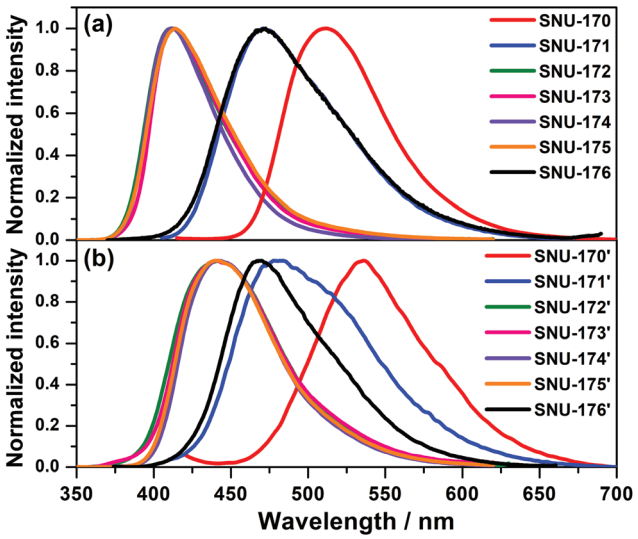

Fig. 3 Photoluminescence spectra of MOFs. (a) As-synthesized samples; excitation at 400 nm for **SNU-170**, 390 nm for **SNU-171**, 350 nm for **SNU-176**, and 330 nm for the rest of the samples. (b) After supercritical CO_2 activation, excitation at 400 nm for **SNU-170′**, 390 nm for **SNU-171′**, 350 nm for **SNU-176′**, and 330 nm for the rest of the samples.

were previously observed for other activated MOFs, and they were explained by the solvent effect of the guest molecules.[27]

As shown in Fig. 4, the PL emission intensity and the emission wavelength of the activated MOF restore upon resolvation. On the addition of a few drops of DMF to the activated **SNU-170′**, the emission band undergoes a blue-shift from 536 nm to 510 nm, and its relative intensity increases to reach the saturation stage in *ca.* 60 min, suggesting a slow structural rearrangement upon resolvation. As shown by the X-ray structures of MOFs, the phenyl ring and the vinyl group of H_2CVB-XR, which are linked by a C–C single bond, are located on the same plane. The planar arrangement leads to the conjugation of the π-electron cloud of a benzene ring with a double

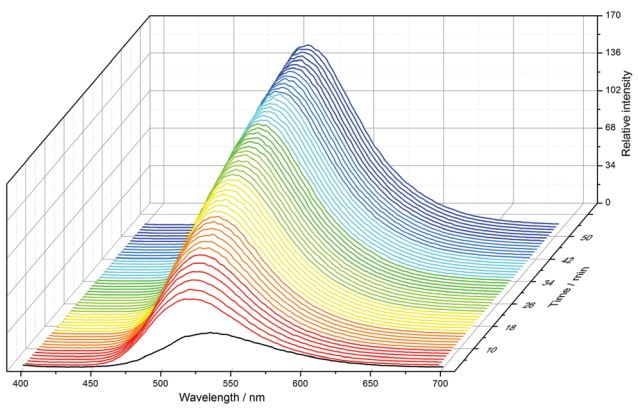

Fig. 4 Time-dependent regeneration of photoluminescence spectra of activated **SNU-170′** upon the addition of a few drops of DMF. Excitation at 380 nm. The black line corresponds to the activated sample of **SNU-170′**.

bond of the vinyl group, which is necessary for luminescence. The planar ligand arrangement is further stabilized in the MOF when the solvent molecules fill the void space. On removal of the guest solvent, the C–C single bond is prone to rotation, which leads to an irregular structure and reduces the degree of π-conjugation in the bulk sample, even though the MOF retains the connectivity of the metal and the ligand. These results are reflected in the PXRD patterns exhibiting the loss of crystallinity (Fig. S9, ESI†) as well as the emission spectra with a remarkable reduction of intensity. The structural changes together with the guest-solvent effect influence the excitation/emission mechanism in the activated MOFs, leading to the dramatic decrease in the emission intensity and the red-shifted emission band. Interestingly, upon resolvation, both the crystallinity as well as photoluminescence is restored, which supports the recovery of the MOF structure and the degree of π-conjugation.

The sensing ability of the MOFs

To see if the present luminescent MOFs can be applied in sensing the types of solvents, we measured the PL spectra of the activated MOFs at room temperature after adding a few drops of DEF, DMA, acetone, benzene, and toluene. With any of these solvents, the luminescence intensities of the activated MOFs increase, and the emission bands show blue shifts (Table S3 and Fig. S14, ESI†). Furthermore, the emission maxima of the MOFs depend on the types of solvents, suggesting their solvent-sensing capability. The non-polar aromatic solvents such as benzene and toluene show the most red-shifted emissions, in particular for **SNU-172′** and **SNU-173′** by 6–10 nm, compared with other solvents, which is in agreement with the previous reports.[26,27] The shifts of the emission maxima depending on the solvents are attributed to the interaction between the ligands of the MOFs and the solvents. The solvents with different polarities and shapes interact differently with the ligands in the MOF pores, leading to the change in the intra-ligand HOMO–LUMO energy gap.[28]

The development of sensing materials to detect the nitro derivatives of organic compounds, which are strong explosives, is important.[18] When a drop of 0.5 M DMF solution of nitrobenzene (NB) or that of 2,4-dinitrotoluene (DNT) is added to the as-synthesized MOFs, the PL emission spectra of **SNU-170–SNU-176** are quenched (Fig. S15, ESI†), implying that the MOFs can sense nitro-organics. The PL quenching must be attributed to the photoinduced electron transfer from the electron-donating ligand to the electron-deficient nitroaromatics upon excitation, which is a deactivation process of PL.[18,29] While the quenched PL spectra of **SNU-170–SNU-175** upon the addition of NB and DNT solutions show no noticeable difference, those of **SNU-176** show a small difference between NB and DNT in the peak positions; λ_{max} = 469 nm for NB and 467 nm for DNT (Fig. S16, ESI†). This suggests that the judicious selection and introduction of multiple ligands to a MOF may be a good strategy for developing MOF materials that not only detect the general nitro-organics, but also pinpoint the target compounds.

Conclusions

We have synthesized multifunctional MOFs that exhibit high gas uptake capacities, photoluminescence, and chemical sensing abilities by utilizing asymmetric dicarboxylic acids having various organic functional pendants on the aryl moiety. The pendant functional groups of the ligands affect the interpenetration of the MOFs. They increase the gas-sorption capacities and the isosteric heats of adsorption for H_2, CO_2, and CH_4 gases. They provide ligand-based photoluminescence and chemical sensing abilities to the MOFs: all as-synthesized MOFs can sense nitroaromatics as shown by luminescence quenching and some activated MOFs can sense solvents as shown by the altered emission maxima with enhanced intensity. Interestingly, the MOF **SNU-176** composed of two different ligands shows the highest gas uptake capacities among the present MOFs. It also shows the ability to differentiate nitrobenzene (NB) and 2,4-dinitrotoluene (DNT), unlike the MOFs composed of single ligands. This work shows a strategy to generate and fine-tune the multi-functionality of MOFs by the judicious introduction of functional groups in the ligand. It also suggests that the MOFs synthesized from multiple ligands having selected functional pendants would provide the enhanced functionalities that the MOFs prepared from the single ligand cannot.

Experimental

General methods

All chemicals were commercially available reagent grade and were used without further purification. IR spectra were recorded using a PerkinElmer Spectrum One FTIR spectrophotometer. UV-Visible and diffuse reflectance spectra were measured using a PerkinElmer Lambda 35 UV/Vis spectrometer. Photoluminescence spectra were measured using a PerkinElmer LS-55 luminescence spectrometer. Elemental analyses were performed using a PerkinElmer 2400 Series II CHN analyzer. Thermogravimetric analysis (TGA) was performed using the TGA Q50 TA instruments under a N_2 atmosphere at a scan rate of 5 °C min^{-1} (Fig. S17–S23, ESI†). NMR spectra were measured using a Bruker Spectrospin 300 spectrometer. Powder X-ray diffraction (PXRD) data were recorded using a Bruker D8 Advance diffractometer operating at 40 kV and 40 mA and employing Cu-Kα (λ = 1.54050 Å) with a scan speed of 0.2 s per step and a step size of 0.02 in 2θ.

Synthesis of ligands

A series of substituted 4-(2-carboxyvinyl)benzoic acids with various functional groups (–NH_2, –SMe, –OMe, –OEt, –OPr, and –OBu) was prepared by modifying the reported synthetic methods (see the ESI† for the details of synthetic procedures and characterization data). The ligands obtained were characterized by elemental analyses, FTIR spectroscopy, and ^{1}H NMR spectroscopy.

Synthesis of MOFs

Synthesis of $[Zn_4O(CVB\text{-}NH_2)_3]\cdot 18DMF\cdot H_2O$ (SNU-170). $Zn(NO_3)_2\cdot 6H_2O$ (0.060 g, 0.201 mmol) and $H_2CVB\text{-}NH_2$ (0.021 g, 0.101 mmol) were dissolved in *N*,*N*-dimethylformamide (5 mL) in a glass serum bottle, which was capped with a silicon stopper and aluminium seal, and then heated at 105 °C for 24 h in a programmable furnace. Yellow cubic shaped crystals were formed, which were filtered, washed with DMF, and stored in DMF. Yield: 0.040 g (54%). Anal. calcd for $C_{84}H_{149}N_{21}O_{32}Zn_4$: C, 45.31; H, 6.74; N, 13.21. Found: C, 44.50; H, 6.96; N, 13.78. FTIR (KBr pellet): $\tilde{\nu}$ = 2927 (amino), 1671 cm^{-1} (DMF).

Synthesis of SNU-171–SNU-176. The MOFs were synthesized by using the corresponding $H_2CVB\text{-}XR$ by a method similar to that used for the synthesis of $[Zn_4O(CVB\text{-}NH_2)_3]\cdot 18DMF\cdot H_2O$ (**SNU-170**). The characterization data are provided in the ESI.†

X-ray crystallography

X-ray single-crystal data were collected using an ADSC Quantum-210 detector at 2D SMC with a silicon (111) double crystal monochromator at the Pohang Accelerator Laboratory, Korea. Each crystal was sealed in a glass capillary together with DMF and the data were collected at 293 K. The ADSC Q210 ADX program[30] was used for data collection and HKL3000 sm[31] was used for cell refinement, reduction, and absorption corrections. The structure was solved using SHELXS-2013[31] and full-matrix least-squares refinement against F^2 was carried out using SHELXL-2013.[32] All hydrogen atoms were assigned based on geometrical considerations and allowed to ride on the respective carbon atoms. The solvent molecules could not be located from the difference maps, and the residual electron density corresponding to the solvent molecules was ignored by using the SQUEEZE[33] option of PLATON.[34] The pendant groups and the central benzene ring in the dicarboxylic acids have a high thermal disorder as the structures were solved by using the data collected at 293 K. The X-ray diffraction analysis at 100 K could not be performed due to poor diffraction profiles. The positions of the carbon atoms of the ligand were fixed and refined isotropically and the exact positions of the pendent groups could not be located from the difference map particularly due to the asymmetric dicarboxylate ligand and the flexibility of the pendant groups. Therefore, the number of guest solvent molecules was calculated from the elemental and thermogravimetric analyses data. The X-ray crystallographic data are provided in Table S1, ESI.†

Methods

Activation of MOFs with supercritical CO_2. The crystals of the as-synthesized MOFs (*ca.* 0.1 g) were placed in a supercritical dryer together with DMF, and the drying chamber was sealed. The temperature and pressure of the chamber were increased to 40 °C and 200 bar with CO_2, respectively. The chamber was vented at a rate of 10 mL min^{-1} and then filled with CO_2 again. The cycle of refilling with CO_2, pressurizing, and then venting was repeated for 24 h. After drying, the

closed container was transferred to a glove bag filled with argon and the sample was transferred to a gas sorption cell. The gas sorption isotherms were measured after the samples were evacuated under high vacuum. **SNU-170′**: Anal. calcd for $[Zn_4O(CVB\text{-}NH_2)_3]$ ($C_{30}H_{21}N_3O_{13}Zn_4$): C, 40.35; H, 2.37; N, 4.71. Found: C, 39.54; H, 2.83; N, 4.55. **SNU-171′**: Anal. calcd for $[Zn_4O(CVB\text{-}SMe)_3]$ ($C_{33}H_{24}O_{13}S_3Zn_4$): C, 40.19; H, 2.45. Found: C, 38.84; H, 2.84. **SNU-172′**: Anal. calcd for $[Zn_4O(CVB\text{-}OMe)_3]$ ($C_{33}H_{24}O_{16}Zn_4$): C, 42.25; H, 2.58. Found: C, 41.77; H, 2.68. **SNU-173′**: Anal. calcd for $[Zn_4O(CVB\text{-}OEt)_3]$ ($C_{36}H_{30}O_{16}Zn_4$): C, 44.11; H, 3.08. Found: C, 42.68; H, 3.55. **SNU-174′**: Anal. calcd for $[Zn_4O(CVB\text{-}OPr)_3]$ ($C_{39}H_{36}O_{16}Zn_4$): C, 45.82; H, 3.55. Found: C, 44.84; H, 3.97. **SNU-175′**: Anal. calcd for $[Zn_4O(CVB\text{-}OBu)_3]$ ($C_{42}H_{42}O_{16}Zn_4$): C, 47.40; H, 3.98. Found: C, 44.98; H, 4.37. **SNU-176′**: Anal. calcd for $[Zn_4O(CVB\text{-}SMe)_1(CVB\text{-}OMe)_2]$ ($C_{33}H_{24}O_{15}SZn_4$): C, 41.54; H, 2.54. Found: C, 38.51; H, 2.97.

Measurements of gas sorption data. Gas adsorption–desorption measurements were performed by using Autosorb-1 or Autosorb-3B (Quantachrome Instruments) up to 1 atm. All gases used in the studies were of 99.999% purity. Before and after the gas sorption measurement, the sample weight was measured precisely.

Calculation of the isosteric heat of H_2 adsorption. The isosteric heat of H_2 adsorption was estimated from the adsorption data measured at 77 and 87 K. These data were fit into a virial-type expression (1) by using the R-Program[35] in which, a_i and b_i are temperature independent parameters, P is the pressure (atm), N is the amount of adsorbed H_2 gas (mg g^{-1}), T is the temperature (K), and m and n represent the number of coefficients required to adequately describe the isotherms. The isosteric heat of H_2 adsorption (Q_{st}) was

$$\ln P = \ln N + \frac{1}{T}\sum_{i=0}^{m} a_i N^i + \sum_{i=0}^{n} b_i N^i \quad (1)$$

$$Q_{st} = -R\sum_{i=0}^{m} a_i N^i \quad (2)$$

$$N = \frac{N_m \times b \times P^{(1/c)}}{1 + b \times P^{(1/c)}} \quad (3)$$

$$(\ln P)_N = -\frac{Q_{st}}{R}\frac{1}{T} + C \quad (4)$$

calculated using eqn (2), where R is the universal gas constant.

Calculation of isosteric heats of CO_2 and CH_4 adsorption. The CO_2 and CH_4 gas adsorption isotherms at 195, 273, and 298 K were fitted with a Langmuir–Freundlich equation (eqn (3)). The isosteric heats of CO_2 and CH_4 adsorption were calculated from the Langmuir–Freundlich fitted isotherms by using the Clausius–Clapeyron expression (4), in which, P is the pressure (atm), N is the amount of adsorbed gas (mmol g^{-1}), N_m is the amount of adsorbed gas at saturation, and b and c are constants.

Calculation of CO_2 separation parameters for the vacuum swing adsorption (VSA) method. For evaluation of the materials for the separation of CO_2 from CH_4 and N_2, Bae and Snurr[23] suggested the use of five parameters: (1) CO_2 uptake under the adsorption conditions, N_1^{ads} (mol kg^{-1}), (2) working CO_2 capacity, $\Delta N_1 = N_1^{ads} - N_1^{des}$ (mol kg^{-1}), (3) regenerability, $R = (\Delta N_1/N_1^{ads}) \times 100$ (%), (4) selectivity under adsorption conditions, $\alpha_{12}^{ads} = (N_1^{ads}/N_2^{ads})(y_2/y_1)$, and (5) sorbent selection parameter, $S = (\alpha_{12}^{ads})^2/(\alpha_{12}^{des})(\Delta N_1/\Delta N_2)$. Here N is the adsorbed amount and y is the mole fraction in the gas phase. Subscripts 1 and 2 indicate the strongly adsorbed component (CO_2) and the weakly adsorbed component (CH_4 or N_2), respectively. The selectivity parameters were extracted from the isotherms of CO_2, CH_4, and N_2 at 298 K, which were fit to the Langmuir–Freundlich equation (eqn (3)). The results are presented in Table S2, ESI.†

Conflicts of interest

There are no conflicts to declare.

Acknowledgements

This work was supported by the National Research Foundation of Korea (NRF) Grant funded by the Korean Government (MEST; no. 2005-0049412).

Notes and references

1 E. D. Bloch, W. L. Queen, M. R. Hudson, J. A. Mason, D. J. Xiao, L. J. Murray, R. Flacau, C. M. Brown and J. R. Long, *Angew. Chem., Int. Ed.*, 2016, **55**, 8605–8609.
2 S. Abednatanzi, P. G. Derakhshandeh, H. Depauw, F. X. Coudert, H. Vrielinck, P. Van Der Voort and K. Leus, *Chem. Soc. Rev.*, 2019, **48**, 2535–2565.
3 H. Bunzen, F. Kolbe, A. Kalytta-Mewes, G. Sastre, E. Brunner and D. Volkmer, *J. Am. Chem. Soc.*, 2018, **140**, 10191–10197.
4 M. P. Suh, H. J. Park, T. K. Prasad and D. W. Lim, *Chem. Rev.*, 2012, **112**, 782–835.
5 D. W. Lim, S. A. Chyun and M. P. Suh, *Angew. Chem., Int. Ed.*, 2014, **53**, 7819–7822.
6 D. W. Lim, J. W. Yoon, K. Y. Ryu and M. P. Suh, *Angew. Chem., Int. Ed.*, 2012, **51**, 9814–9817.
7 J. M. Yu, L. H. Xie, J. R. Li, Y. G. Ma, J. M. Seminario and P. B. Balbuena, *Chem. Rev.*, 2017, **117**, 9674–9754.
8 D. H. Hong and M. P. Suh, *Chem. – Eur. J.*, 2014, **20**, 426–434.
9 A. Bavykina, N. Kolobov, I. S. Khan, J. A. Bau, A. Ramirez and J. Gascon, *Chem. Rev.*, 2020, **120**, 8468–8535.
10 K. Cho, S. H. Han and M. P. Suh, *Angew. Chem., Int. Ed.*, 2016, **55**, 15301–15305.
11 A. Dhakshinamoorthy, Z. H. Li and H. Garcia, *Chem. Soc. Rev.*, 2018, **47**, 8134–8172.
12 Y. M. Zhang, S. Yuan, G. Day, X. Wang, X. Y. Yang and H. C. Zhou, *Coord. Chem. Rev.*, 2018, **354**, 28–45.

13 W. P. Lustig, S. Mukherjee, N. D. Rudd, A. V. Desai, J. Li and S. K. Ghosh, *Chem. Soc. Rev.*, 2017, **46**, 3242–3285.
14 L. E. Kreno, K. Leong, O. K. Farha, M. Allendorf, R. P. Van Duyne and J. T. Hupp, *Chem. Rev.*, 2012, **112**, 1105–1125.
15 Y. X. Tan, F. Wang and J. Zhang, *Chem. Soc. Rev.*, 2018, **47**, 2130–2144.
16 Q. Xia, H. Wang, B. Huang, X. Yuan, J. Zhang, J. Zhang, L. Jiang, T. Xiong and G. Zeng, *Small*, 2019, **15**, e1803088.
17 J. Wang, J. Wu, L. Lu, H. Xu, M. Trivedi, A. Kumar, J. Liu and M. Zheng, *Front. Chem.*, 2019, **7**, 244.
18 Z. C. Hu, B. J. Deibert and J. Li, *Chem. Soc. Rev.*, 2014, **43**, 5815–5840.
19 H. J. Park, D. W. Lim, W. S. Yang, T. R. Oh and M. P. Suh, *Chem. – Eur. J.*, 2011, **17**, 7251–7260.
20 H. J. Park and M. P. Suh, *Chem. Sci.*, 2013, **4**, 685–690.
21 S. Sung and M. P. Suh, *J. Mater. Chem. A*, 2014, **2**, 13245–13249.
22 T. K. Prasad and M. P. Suh, *Chem. – Eur. J.*, 2012, **18**, 8673–8680.
23 Y. S. Bae and R. Q. Snurr, *Angew. Chem., Int. Ed.*, 2011, **50**, 11586–11596.
24 O. V. Ershov, M. Y. Ievlev, M. Y. Belikov, A. I. Naidenova, V. N. Maksimova and V. A. Tafeenko, *RSC Adv.*, 2017, **7**, 34886–34891.
25 X. Li, X. W. Wang and Y. H. Zhang, *Inorg. Chem. Commun.*, 2008, **11**, 832–834.
26 F. Drache, V. Bon, I. Senkovska, M. Adam, A. Eychmüller and S. Kaskel, *Eur. J. Inorg. Chem.*, 2016, 4483–4489.
27 R. Zou, X. Ren, F. Huang, Y. Zhao, J. Liu, X. Jing, F. Liao, Y. Wang, J. Lin, R. Zou and J. Sun, *J. Mater. Chem. A*, 2015, **3**, 23493–23500.
28 F.-Y. Yi, D. Chen, M.-K. Wu, L. Han and H.-L. Jiang, *ChemPlusChem*, 2016, **81**, 675–690.
29 M. Pamei and A. Puzari, *Nano-Struct. Nano-Objects*, 2019, **19**, 100364; T. K. Kim, J. H. Lee, D. Moon and H. R. Moon, *Inorg. Chem.*, 2013, **52**, 589–595.
30 A. J. Arvai and C. Nielsen, *ADSC Quantum-210 ADX Program*, Area Detector System Corporation, Poway, CA, USA, 1983.
31 Z. Otwinowski and W. Minor, in *Methods in Enzymology*, ed. C. W. Carter Jr. and R. M. Sweet, Academic Press, New York, 1997, vol. 276((Part A)), p. 307.
32 G. M. Sheldrick, *SHELX-2013-Programs for Crystal Structure Analysis*, Institüt für Anorganische Chemie der Universität, Tammanstrasse 4, D-3400 Göttingen, Germany, 1998.
33 P. v. d. Sluis and A. L. Spek, *Acta Crystallogr., Sect. A: Found. Crystallogr.*, 1990, **46**, 194–201.
34 (*a*) A. L. Spek, *Acta Crystallogr., Sect. A: Found. Crystallogr.*, 1990, **46**, C34; (*b*) A. L. Spek, *PLATON, A Multipurpose Crystallographic Tool*, Utrecht University, Utrecht, The Netherlands, 1998.
35 L. Czepirski and J. Jagiello, *Chem. Eng. Sci.*, 1989, **44**, 797–801.

